JOURNAL OF GEOPHYSICAL RESEARCH, VOL. 102, NO. E7, PAGES 16,339–16,359, JULY 25, 1997

A 70th degree lunar gravity model (GLGM-2) from Clementine and other tracking data

Frank G. R. Lemoine, David E. Smith, Maria T. Zuber,[1] Gregory A. Neumann,[1] and David D. Rowlands

Laboratory for Terrestrial Physics, NASA Goddard Space Flight Center, Greenbelt, Maryland

Abstract. A spherical harmonic model of the lunar gravity field complete to degree and order 70 has been developed from S band Doppler tracking data from the Clementine mission, as well as historical tracking data from Lunar Orbiters 1-5 and the Apollo 15 and 16 subsatellites. The model combines 361,000 Doppler observations from Clementine with 347,000 historical observations. The historical data consist of mostly 60-s Doppler with a noise of 0.25 to several mm/s. The Clementine data consist of mostly 10-s Doppler data, with a data noise of 0.25 mm/s for the observations from the Deep Space Network, and 2.5 mm/s for the data from a naval tracking station at Pomonkey, Maryland. Observations provided Clementine, provide the strongest satellite constraint on the Moon's low-degree field. In contrast the historical data, collected by spacecraft that had lower periapsis altitudes, provide distributed regions of high-resolution coverage within ±29° of the nearside lunar equator. To obtain the solution for a high-degree field in the absence of a uniform distribution of observations, we applied an a priori power law constraint of the form $15 \times 10^{-5}/l^2$ which had the effect of limiting the gravitational power and noise at short wavelengths. Coefficients through degree and order 18 are not significantly affected by the constraint, and so the model permits geophysical analysis of effects of the major basins at degrees 10-12. The GLGM-2 model confirms major features of the lunar gravity field shown in previous gravitational field models but also reveals significantly more detail, particularly at intermediate wavelengths (10^3 km). Free-air gravity anomaly maps derived from the new model show the nearside and farside highlands to be gravitationally smooth, reflecting a state of isostatic compensation. Mascon basins (including Imbrium, Serenitatis, Crisium, Smythii, and Humorum) are denoted by gravity highs first recognized from Lunar Orbiter tracking. All of the major mascons are bounded by annuli of negative anomalies representing significant subsurface mass deficiencies. Mare Orientale appears as a minor mascon surrounded by a horseshoe-shaped gravity low centered on the Inner and Outer Rook rings that is evidence of significant subsurface structural heterogeneity. Although direct tracking is not available over a significant part of the lunar farside, GLGM-2 resolves negative anomalies that correlate with many farside basins, including South Pole-Aitken, Hertzsprung, Korolev, Moscoviense, Tsiolkovsky, and Freundlich-Sharonov.

Introduction

Until the launch of Clementine, on January 24, 1994, the sources of tracking data for gravity models derived by U.S. investigators have been the Lunar Orbiters and the Apollo spacecraft. The Lunar Orbiters were inserted into elliptical orbits with periapses of 50 to 100 km above the lunar surface. The Apollo spacecraft were placed in near circular orbits at low inclinations with a mean altitude of 100 km, although some tracking was acquired from altitudes as low as 10 to 20 km. The tracking data sampled the gravity field of the Moon at a resolution unprecedented for orbiting spacecraft, at either the Earth, Venus, or Mars. However, the spatial coverage of the tracking was incomplete, with no direct tracking data available over large portions of the lunar farside. During the initial investigations, in the 1960s and 1970s, researchers were limited in the size of the spherical harmonic solutions that could be developed by the computers then available. Because of the power

[1]Also at Department of Earth, Atmospheric, and Planetary Sciences, Massachusetts Institute of Technology, Cambridge.

Paper number 97JE01418.
0148-0227/97/97JE-01418$09.00

of the higher degree harmonics in the tracking data, the early solutions encountered severe difficulties with the aliasing of the high-degree signal into the lower degree terms. In an effort to exhaust the available signal in the tracking data, other methods were employed to map the lunar gravity field. These alternate methods included the estimation of discrete masses over the lunar surface, or the mapping of the accelerations experienced by orbiting spacecraft in the line of sight (LOS) between the spacecraft and tracking station.

A selection of the solutions for the lunar gravity field that have been developed since the 1960s is summarized in Table 1. The landmark solutions include those of *Muller and Sjogren* [1968], *Williams et al.* [1973], *Sjogren et al.* [1974a], *Ferrari* [1977], *Bills and Ferrari* [1980], and *Konopliv et al.* [1993]. The analysis of the Lunar Orbiter data by *Muller and Sjogren* [1968] led to the discovery of the mass concentrations ("mascons") under the ringed lunar maria. *Williams et al.* [1973] employed laser ranging to retroflectors left on the lunar surface in combination with lunar gravity solutions derived from radiometric tracking. The lunar laser ranging data are sensitive to the second-degree and third-degree gravity field harmonics, through their influence on the lunar physical librations [*Dickey et al.*, 1994]. *Sjogren et al.* [1974a] used data from the Apollo 15 and 16 subsatellites to map the nearside of the Moon ±29° in latitude and ±100° in longitude, using both LOS accelerations and the estimation of discrete masses on the lunar surface. The Apollo subsatellites marked the first time an extensive amount of data was acquired from a lunar satellite in low-altitude (100 km) near-circular orbit. The command and service modules of the Apollo spacecraft were also located in low-altitude, near-circular orbits. In some cases, these spacecraft came as low as 12 to 20 km from the lunar surface; however, these data were limited spatially and temporally. The data from Apollo missions 8 and 12, in combination with the Lunar Orbiter data, were used by *Wong et al.* [1971] to solve for 600 discrete masses over the nearside (±60° in latitude and ±95° in longitude). Data from Apollo missions 14, 15, 16, 17, were used by *Muller et al.* [1974], and *Sjogren et al.* [1972a,b; 1974b,c] to map the LOS accelerations.

Ferrari [1977] derived mean elements from short-arc fits to the tracking data. *Ferrari* [1977] developed a 16th degree spherical harmonic solution that was among the first to show plausible correlations between a map of surface gravity anomalies and farside lunar features, such as Mendeelev, Korolev, and Moscoviense. *Bills and Ferrari* [1980] combined much of the data used by previous investigators, such as the Lunar Orbiter data, the Apollo data from *Wong et al.* [1971], the tracking of the Apollo 15 and 16 subsatellites, and lunar laser ranging. They developed a 16th degree spherical harmonic solution that remained the best lunar gravity model for the next 13 years.

Konopliv et al. [1993] developed a 60th degree model from the tracking of the Lunar Orbiters and the Apollo subsatellites. Taking advantage of the high speed and memory capacity of more modern computers, this model represented the first realistic attempt to exhaust the gravity signal from the low periapse satellites in a high-degree spherical harmonic solution. This model has excellent performance in terms of its root mean square (RMS) fit to the tracking data, and the map of the

Table 1. Previous Lunar Gravity Analyses

Reference	Data Used	Comment
Muller and Sjogren [1968]	Lunar Orbiters	Discovery of lunar mascons.
Lorell and Sjogren [1968]	Lunar Orbiters	4x4 spherical harmonic solution + zonals to l=8.
Wong et al. [1971]	Apollo 8, 12	Solution for discrete masses on near side.
Michael and Blackshear [1972]	Lunar Orbiters	13x13 spherical harmonic solution.
Sjogren et al. [1972a,b; 1974b,c]; *Muller et al.* [1974]	Apollos 14-17	Mapped line of sight (LOS) accelerations with data from as low as 12-20 km altitude.
Sjogren et al. [1974a]	Apollo subsatellites	Solve for LOS and discrete masses.
Ferrari [1977]	LO-5 and Apollo subsatellites	16x16 spherical harmonic solution.
Ananda [1977]		Solve for discrete masses.
Bryant and Williamson [1974]	Explorer 49	3x3 spherical harmonic solution from Keplerian mean elements.
Blackshear and Gapcynski [1977]	Explorers 35 and 49	Zonal solution, J_2 - J_6 only from Keplerian mean elements.
Williams et al. [1973]	Lunar laser ranging (LLR)	
Ferrari et al. [1980]	LLR and LO-4	
Bills and Ferrari [1980]	LLR, LO 1-5, Apollo subsatellites, and Apollo 8,12	16x16 spherical harmonic solution
Konopliv et al. [1993]	LO 1-5 and Apollo subsatellites	60x60 spherical harmonic solution.
Dickey et al. [1994]	LLR	

lunar gravity anomalies appears smooth when mapped on a surface at 100 km altitude. However, the high-degree terms have excessive power, and when the gravity anomalies are mapped onto the lunar surface, numerous artifacts become apparent, which make the model unsatisfactory for use in geophysical studies. The goal of the new analysis was to develop a lunar gravity model that (1) included both the historical tracking data from the Lunar Orbiters and the Apollo subsatellites, as well as the new data from Clementine; (2) attenuated spurious power in the high-degree terms; and (3) produced a model suitable for use in geophysical studies of the Moon when used in conjunction with the Clementine laser altimeter data.

Data

The data in GLGM-2 consist of the Doppler tracking of the U.S. Lunar Orbiter Satellites 1 to 5 (referred to by shorthand as LO-1, LO-2, etc., for the remainder of this paper), the Apollo 15 and 16 subsatellites, and the Clementine spacecraft. Other data, such as the tracking from the Explorers 35 and 49 and S band tracking from tracking of the Apollo command and service modules, could not be located, even after searches at the National Space Science Data Center (NSSDC), the Jet Propulsion Laboratory (JPL), and the Johnson Space Center (JSC). Explorers 35 and 49 were placed in high lunar orbits, and were sensitive to the low-degree harmonics [*Bryant and Williamson*, 1974; *Gapcynski et al.*, 1975; *Blackshear and Gapcynski*, 1977]. In addition, these spacecraft were tracked by VHF, not S band tracking, and so were noisier because of the increased sensitivity to the ionosphere, and the solar plasma (R. Williamson, personal communication, 1994). Other existing data which might be used include the tracking of the Soviet Luna spacecraft. These spacecraft are located in complementary, frequently higher inclination orbits than the U.S. Lunar Orbiters and the Apollo spacecraft. The analysis of the limited amount of Luna data is discussed by *Sagitov et al.* [1986] but was not pursued in our analysis.

The orbit characteristics of Lunar Orbiter spacecraft and the Apollo subsatellites are summarized in Table 2. In general, the Lunar Orbiters were placed in elliptical orbits about the Moon, with periods of 200 to 210 min. Periapse heights ranged from 30 to 210 km, depending on the mission phase. In addition, periapsis and, consequently, the region of highest resolution was almost always placed near the lunar equator. Lunar Orbiters 1 to 3 had low-inclination orbits (12° to 21°). Lunar Orbiters 4 and 5 had near-polar inclinations of about

Table 2. Orbits of Lunar Spacecraft

Spacecraft	Date	Periapse Height, km	Period min	Semimajor Axis, km	Eccentricity	Inclination deg
Lunar Orbiter 1	Aug. 14, 1966	189	218	2766	0.3031	12.2
	Aug. 21, 1966	57	209	2693	0.3335	12.0
	Aug. 25, 1966	41	206	2670	0.3336	12.1
Lunar Orbiter 2	Nov. 10, 1966	196	218	2772	0.3021	12.0
	Nov. 15, 1966	50	208	2689	0.3353	11.9
	Dec. 8, 1966	43	210	2702	0.3408	17.6
	Apr. 14, 1967	69	209	2693	0.3289	17.2
	June 27, 1967	113	212	2716	0.3184	16.5
	July 24, 1967	98	212	2716	0.3240	16.1
Lunar Orbiter 3	Feb. 9, 1967	210	215	2744	0.2899	21.0
	Feb. 12, 1967	55	209	2689	0.3331	20.9
	Apr. 12, 1967	59	207	2680	0.3294	21.2
	July 17, 1967	144	212	2722	0.3088	21.0
	Aug. 30, 1967	145	131	1968	0.0435	20.9
Lunar Orbiter 4	May 8, 1967	2706	721	6150	0.2773	85.5
	June 6, 1967	75	501	4820	0.6238	84.9
	June 9, 1967	77	344	3753	0.5163	84.4
Lunar Orbiter 5	Aug. 5, 1967	195	505	4852	0.6017	85.0
	Aug. 7, 1967	100	501	4822	0.6185	84.6
	Aug. 9, 1967	100	191	2537	0.2760	84.7
	Oct. 10, 1967	198	225	2832	0.3155	85.2
Apollo 15 subsatellite	Aug. 29, 1971	89	118	1858	0.0167	151.0
Apollo 16 subsatellite	Apr. 27, 1972	73	119	1849	0.0205	169.3
Clementine	Feb. 19, 1994	402	474	4651	0.5400	89.5
	Feb. 21, 1994	398	299	3418	0.3755	89.3
	Feb. 22, 1994	383	299	3414	0.3789	89.4
	Mar. 11, 1994	400	298	3414	0.3738	89.8
	Mar. 27, 1994	447	298	3414	0.3598	90.1
	Apr. 11, 1994	427	298	3415	0.3657	90.0

85°. The Lunar Orbiters were tracked by the antennae of the Deep Space Network (DSN), principally at stations 12 (Goldstone, California), 41 (Canberra, Australia), 61 and 62 (Madrid, Spain). The data consist of mostly 60-s two-way and three-way Doppler, with noise ranging from 0.35 to occasionally as high as 5 mm/s on some arcs.

Each Lunar Orbiter spacecraft had two mission phases: a primary mission devoted to photographic mapping, with intense tracking, and an extended mission with sparser tracking. The attitude control system of the Lunar Orbiters was uncoupled in pitch and yaw, so that each time the spacecraft changed its orientation, a spurious acceleration was imparted to the spacecraft [*Konopliv et al.*, 1993]. The maneuvers were most extensive during the photographic (primary) mission phases but also occurred during the extended missions. The times of these maneuvers are known, so that their effects can be accommodated by estimating three-axis accelerations, radial, along-track, and cross-track to the orbit at the time of the maneuvers. During the photographic missions, as many as 14 sets of attitude maneuvers occurred per day. Maneuvers closely spaced in time were combined, and a single set of acceleration parameters was estimated to account for the attitude-induced orbit perturbations. Also, because of the numerous maneuvers, during the photographic phases of the Lunar Orbiter missions, data arcs were limited to no longer than one day. The LO-3 spacecraft was briefly inserted into a near-circular orbit about the Moon, simulating the orbit planned for the then future Apollo missions; however, sparse tracking limited the amount of data that was returned from this orbit.

The Apollo 15 and Apollo 16 spacecraft deployed subsatellites in lunar orbit. These spacecraft, designed to study the magnetic fields, plasmas, and energetic particles in the vicinity of the Moon, also carred S band transponders to support high-precision gravity mapping of the Moon [*Coleman et al.*, 1972; *Anderson et al.*, 1972a,b]. The spacecraft were spin stabilized and did not use any thrusters to maintain their attitude, making the data much cleaner than the tracking data from the Lunar Orbiters. The two subsatellites were deployed by the Apollo 15 and 16 command modules in near-circular, retrograde orbits of the Moon (inclinations of 152° and 169°). The two spacecraft were tracked by the antennae of the Manned Space Flight Network (MSFN) [*Sjogren et al.*, 1974a]. The spacecraft permitted a uniform mapping of the nearside of the Moon up to about 29°N or S from a mean altitude of 100 km. Unfortunately, the satellites did not use satellite-to-satellite tracking to permit acquisition of data while flying over the lunar farside.

The Clementine spacecraft was launched from Vandenburg Air Force Base on January 24, 1994, and became the first U.S. spacecraft to return to lunar orbit in almost 20 years [*Nozette et al.*, 1994]. Clementine carried an S band transponder suitable for gravity mapping and was placed into an elliptical orbit about the Moon, with a period of approximately 300 min and a mean periapsis altitude of 415 km. Unlike the Lunar Orbiters, whose orbit periapses were close to the lunar equator, for Clementine the periapsis was located near 30°S during the first month of mapping, and near 30°N during the second month in lunar orbit. Clementine was tracked by the 26-m and 34-m antennae of the DSN, as well as by the 30-m Pomonkey antenna operated by the Naval Research Laboratory in southern Maryland. The data from Clementine were predominantly two-way Doppler, averaged over 10 s. The noise of the DSN data averaged 0.25 to 0.30 mm/s, whereas the noise of the Pomonkey data typically ranged from 2.5 to 3.0 mm/s. Clementine remained in orbit about the Moon from February 19 to May 4, 1994. Nearly all the available Clementine tracking data from the DSN and Pomonkey were used in GLGM-2.

The available tracking data constrain the global gravity field of the Moon at moderate resolution and provide higher resolution coverage in the equatorial regions. The Doppler data available below 500 km are illustrated in Figure 1. It is evident from these figures that lunar librations and parallax allow direct tracking of spacecraft over the poles to 60°N or S on the farside and to ±120° longitude, where 0° longitude is the meridian at the center of the nearside.

Method of Solution

Definition

The lunar gravity potential, U, is modeled in spherical harmonics using the expression,

$$U = \frac{GM}{r}\sum_{l=0}^{\infty}\left(\frac{a_e}{r}\right)^l \sum_{m=0}^{l}\{\bar{C}_{lm}\cos m\lambda + \bar{S}_{lm}\sin m\lambda\}\bar{P}_{lm}(\sin\phi) \qquad (1)$$

where the expansion is defined in spherical coordinates with radius r, latitude ϕ, and longitude λ; $\bar{C}_{lm}$ and $\bar{S}_{lm}$ represent the normalized geopotential coefficients; $\bar{P}_{lm}$ are the normalized associated Legendre functions of degree l and order m; a_e is the reference equatorial radius; G is the universal constant of gravitation, and M is the lunar mass. In a coordinate system whose origin coincides with the center of mass, the degree one terms of equation (1) vanish.

The geopotential coefficients may be unnormalized by the following relation [*Kaula*, 1966],

$$C_{lm} = \left[\frac{(l-m)!\,(2l+1)\,(2-\delta_{0m})}{(l+m)!}\right]^{\frac{1}{2}}\bar{C}_{lm} \qquad (2)$$

where δ_{0m} is the Kronecker delta ($\delta_{0m} = 0$ for $m \neq 0$, and $\delta_{0m} = 1$ for $m=0$), and the equation can apply to $\bar{C}_{lm}$ or $\bar{S}_{lm}$. A solution for the lunar gravity field consists of an estimate for the lunar GM, as well as the parameters C_{lm} and S_{lm}. It is frequently convenient to refer to the total amplitude, J_{lm}, of a C_{lm} and S_{lm} coefficient pair, where $J_{lm} = \sqrt{C_{lm}^2 + S_{lm}^2}$.

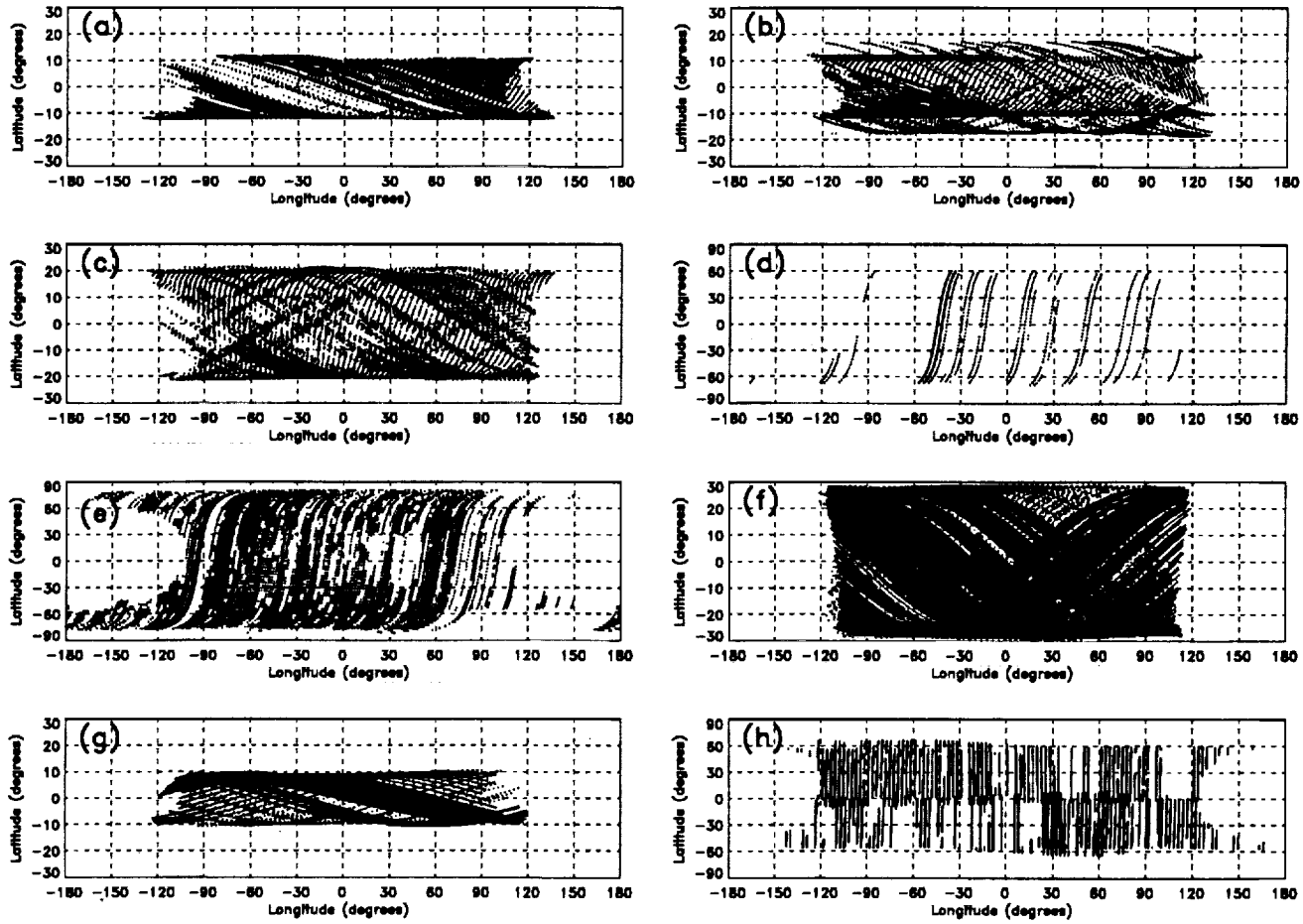

Figure 1. Doppler data coverage below 500 km altitude in GLGM-2 for (a) Lunar Orbiter 1, (b) Lunar Orbiter 2, (c) Lunar Orbiter 3, (d) Lunar Orbiter 4, (e) Lunar Orbiter 5, (f) the Apollo 15 subsatellite, (g) the Apollo 16 subsatellite, and (h) Clementine.

Processing of the Tracking Data

The data were divided into independent data spans, known as arcs, based on knowledge of the spacecraft orbit characteristics, frequency of maneuvers, and availability of tracking data. The GLGM-2 solution was based on 392 arcs, from 6 hours to 12 days in length, and included 708,854 observations, of which 361,794 were contributed by Clementine. For each orbital arc the adjusted parameters included the orbital state, and a single solar radiation pressure coefficient. To account for the spurious accelerations induced by the attitude control systems on the Lunar Orbiters and on some Clementine arcs, three axis accelerations, radial, along-track, and cross-track to the orbit were also estimated. Doppler range-rate biases were estimated for each station in each orbital arc to account for any residual modeling error, such as frequency offsets, errors in the station locations, and imprecise modeling of the troposphere and the ionosphere.

The force model included the third-body perturbations of the Earth, the Sun, and all the planets, the solar radiation pressure, the Earth-induced and solar-induced lunar tides. A k_2 Love number of 0.027, as derived by *Williams et al.* [1987], was applied. The DSN station coordinates were derived from *Folkner* [1993] and mapped back to the 1960s and 1970s using station velocities derived by the *International Earth Rotation Service (IERS)* [1994]. The *Hopfield* [1971] model was applied to correct the tracking data for tropospheric refraction using the mean meteorological data for the DSN sites from *Chao* [1974]. The coordinates of the MSFN stations were initially provided by A. S. Konopliv (personal communication, 1993), and these station positions were adjusted in the global gravity solution. The coordinates of the Earth tracking stations were corrected for the displacement due to the solid tide and ocean loading, although the latter is a small effect for these data. The appropriate relativistic perturbations are applied in the force model and the measurement model. These include the Schwarzschild effect, or the relativistic modification of the central body term, the transformations from coordinate time to atomic time as derived by *Moyer* [1981], and the modification of the ray path due to relativity [*Moyer*, 1971]. We used the 1991 International Astronomical Union (IAU) model [*Davies et al.*, 1992] and the DE200 lunar and planetary ephemerides [*Standish*, 1990]. The *Davies et al.* [1992] reference has a typographical error in Table II (p. 381) that describes the lunar orientation: the parame-

ters defining E3 and E5 should read: E3 = 260.008°+ 13.012001 d, and E5 = 357.529°+ 0.985600 d (M. E. Davies, personal communication, 1993).

Derivation of the Spherical Harmonic Solutions

The GEODYN orbit determination program was used to process the lunar tracking data [*Pavlis et al.*, 1997]. This program has previously been used to process interplanetary tracking data from Mars and Venus [*Smith et al.*, 1993; *Nerem et al.*, 1993]. GEODYN was used to converge the orbital arcs and create the normal equations for the least squares solution. A companion program to GEODYN, SOLVE [*Ullman*, 1994], was used to derive the least squares solution. The normal equations were grouped by satellite, spacecraft mission phase, and orbital geometry. In selecting the a priori weights for each set of data, consideration was given to the apparent data noise (as deduced from analysis of the residuals on a pass by pass basis), the periapse altitude, the length of the data arc, the number of acceleration parameters in an arc, and mission phase. Inspection of the maps of the free-air gravity anomalies also played a role in the selection of the weights. Sets of data that produced spurious signals were rejected or downweighted. Through inspection of the anomaly maps and other tests, arcs with a high data noise (for instance, the LO-5 arcs from August 22-26, 1967) were downweighted. Data from LO-2 for December 1-6, 1966, and for LO-3 from February 28 to March 8, 1967, received close scrutiny. In both instances, tracking was nearly continuous, except for occultation behind the limb of the Moon. This should not be an issue, except that periapse was precessing west out of direct view from Earth, and reached a minimum of 28-km altitude in the case of LO-2, and 38 km in the case of LO-3. In both cases, the proximity of periapsis to the surface, out of view of the direct tracking from Earth, causes powerful perturbations in the tracking data and, ultimately, an indeterminacy in the location of gravity anomalies along the LO-2 and LO-3 ground track on the farside. The result is striping in the maps of the free air gravity anomalies, particularly in the vicinity of Korolev. Downweighting of the data and processing the LO-2 and LO-3 data over this period in short (12-hour) arcs mitigates but does not eliminate these artifacts in the farside anomaly maps.

In order to obtain a solution, it is necessary to solve a least squares system of equations of the form [*Lawson and Hanson*, 1974]

$$Ax = B \tag{3}$$

where A is the set of normal equations, x is a vector representing the deviation of the coefficients from their a priori values $\bar{X}$, and B is the residual vector. Unfortunately, the lunar tracking data are nonuniform in both spatial resolution and distribution. As a consequence, it is not possible to obtain a solution directly, and an a priori constraint must be applied. One approach is to apply a constraint such that

$$(A + \bar{P}^{-1})x = B - \bar{P}^{-1}\bar{X} \tag{4}$$

The diagonal elements of the a priori covariance matrix, $\bar{P}$, have the form

$$\bar{P}_l = \hat{\sigma}_l^2 \tag{5}$$

and

$$\hat{\sigma}_l = K\frac{10^{-5}}{l^2} \tag{6}$$

where K is a scaling factor. *Ferrari* [1977] applied this constraint with $\hat{\sigma}_l = 35 \times 10^{-5}/l^2$, and *Konopliv et al.* [1993] used $\hat{\sigma}_l = 15 \times 10^{-5}/l^2$. *Bills and Ferrari* [1980] used a slightly different power law of the form, such that

$$\bar{P}_l = \frac{1.4 \times 10^{-6}}{(2l+1)^2(l)(l+1)} \tag{7}$$

which, they argued, did not overestimate the low-degree variances, as did the a priori power law used by *Ferrari* [1977]. The application of these sorts of constraints on the total spectral power of the coefficients by degree prevents the high-degree terms from developing excessive power and allows a 70x70 solution to be obtained. One difficulty with the application of this Kaula-like power constraint is the selection of the appropriate multiplier in the power law. For the Earth, independent surface gravity measurements contrain the amplitude of the power spectrum, whereas no such information is available for the Moon. Furthermore, a tight constraint will mute the magnitude of the gravity anomalies, whereas a weaker constraint might allow more "real" power into the anomalies on the nearside, at the expense of inducing spurious high frequency variations on the farside. A variant of this approach was developed by *Konopliv and Sjogren* [1994] and applied to global solutions for the gravity fields of Venus and Mars [*Konopliv and Sjogren*, 1994, 1995]. Their technique involves applying a power law constraint both spatially and spectrally. This is accomplished by writing observation equations on a global basis such that the anomalies on the surface beyond a certain degree are zero to within a prescribed sigma, determined from Kaula's rule. Since we wished to mute the high frequency excursions in the gravity anomalies, we preferred the constraint $\hat{\sigma}_l = 15 \times 10^{-5}/l^2$, although we did test solutions with weaker Kaula constraints, such as $\hat{\sigma}_l = 30 \times 10^{-5}/l^2$, and $\hat{\sigma}_l = 60 \times 10^{-5}/l^2$. A detailed analysis using the spatial and spectral approach was beyond the scope of this study, but a comparison of this method as well as an eigenvalue technique for stabilization for sparse matrices is a current subject of investigation [*Lemoine et al.*, 1996].

In the course of deriving our final spherical harmonic solution, we developed a number of interim solutions to evaluate our results. Some of the fields that we discuss in this paper and their relationship to GLGM-2 are described in Table 3. The data used in the derivation of GLGM-2 are summarized in Table 4.

Calibration of GLGM-2

Once all the data had been processed and assembled into the appropriate set of normal equations, we calibrated the final solution using the method of *Lerch* [1991]. This method involves deriving subset solutions,

Table 3. Lunar Gravity Solutions and Their Relationship to GLGM-2

Solution[a]	Maximum	Description
LUN60D	60x60	*Konopliv et al.* [1993] a priori solution.
GLGM-1	70x70	Predecessor to GLGM-2, from *Lemoine et al.* [1994]. Does not include Apollo 16 subsatellite data. Clementine data weighted at 0.5 cm/s. Solution not calibrated.
LGM-261	70x70	Solution from Clementine data only.
LGM-296a	70x70	New baseline solution prior to calibration.
GLGM-2	70x70	Final calibrated solution from this paper (LGM-309a).
LGM-309b	70x70	Same as GLGM-2, but uses power law constraint of $30 \times 10^{-5}/l^2$.
LGM-309c	30x30	Same data as GLGM-2, but with no power law constraint.
LGM-309d	70x70	Same as GLGM-2, but with no Clementine data.

[a] Unless otherwise noted, all solutions used the a priori power law constraint of $15 \times 10^{-5}/l^2$.

where a single constituent set of data is removed from the nominal solution. The objective of the calibration procedure is to adjust the initial data weight so that the aggregate differences of the coefficients between the subset and the master solution are the same as the aggregate differences between the coefficient sigmas in the subset and the master solution. The objective is to derive a covariance matrix that more closely reflects the intrinsic uncertainties in the data. This procedure has been used extensively to calibrate the covariance matrices of Earth gravity models [*Marsh et al.*, 1988a, 1990; *Nerem et al.*, 1994] and was also applied in the development of GMM-1, a 50th degree and order solution for Mars [*Smith et al.*, 1993].

The calibration factor for each spherical harmonic degree is computed according to the following relation from *Lerch* [1991]:

$$K_l = \left[\frac{\sum_{m=0}^{l} (G_{lm} - \bar{G}_{lm})^2}{\sum_{m=0}^{l} (\bar{\sigma}_{lm}^2 - \sigma_{lm}^2)} \right]^{1/2} \tag{8}$$

where G_{lm} refers to both the C_{lm} and S_{lm} coefficients from the master solution, $\bar{G}_{lm}$ refer to the coefficients from the subset solution, and σ_{lm} and $\bar{\sigma}_{lm}$ refer to the coefficient sigmas from the master and the subset solutions, respectively.

The average calibration factor for a set of data is simply the average over some span of degrees l up to $l_{\max}$, or

$$\bar{K} = \sum_{l=2}^{l_{\max}} \frac{K_l}{l_{\max} - 1} \tag{9}$$

The parameter $\bar{K}$ defines the new scale factor for the normal equations of the set of data whose weights we wish to adjust. The summation is truncated at an intermediate degree, $l_{\max}$, which is usually not the maximum degree of the gravity solution. The calibration factors for the high-degree terms may not be meaningful, since these terms are dominated by the Kaula constraint rather than from the tracking data [*Marsh et al.*, 1988b]. The normal equations are then rescaled by the relation

$$W' = \frac{W}{K^2} \tag{10}$$

and the a priori sigma on the test set of data is related to the weight in the normal equation by the equation,

Table 4. Doppler Data Used in GLGM-2

Spacecraft	Number of Arcs	Average Arc Length, hrs	Total Number of Observations
Lunar Orbiter 1	48	21.76	44,503
Lunar Orbiter 2	75	16.38	76,421
Lunar Orbiter 3	55	17.77	54,163
Lunar Orbiter 4	11	70.16	48,734
Lunar Orbiter 5	51	33.74	47,690
Apollo 15 subsatellite	81	16.76	44,096
Apollo 16 subsatellite	35	4.55	31,453
Clementine	36	44.16	361,794
Total	392		708,854

$$\sigma_o = \frac{1}{\sqrt{W}} \tag{11}$$

If the initial weight has been appropriately selected, then the constant of proportionality $\bar{K}$ should be close to unity. A constant $\bar{K}$ greater than unity indicates that the test set of data should be downweighted in the least squares solution, and a value less than unity indicates the data should receive more weight or emphasis in the least squares solution. Each independent set of data that contributes to the gravity solution may be calibrated in this fashion. The new set of weights is then used to produce the final calibrated solution.

Given the number of independent orbits, a strict application of the calibration technique from *Lerch* [1991] would have required the calculation of an inordinate number of master and subset solutions. Therefore, to simplify the process, the data were divided into 11 manageable sets, based upon satellite and orbit geometry. The data from Lunar Orbiter 5, Clementine, the Apollo subsatellites, and Lunar Orbiter 1 were calibrated individually by satellite. For Lunar Orbiters 2, 3, and 4 the calibration sets were selected based on inclination (in the case of LO-2), eccentricity (in the case of LO-3), and periapse height (for LO-4). The relative data weights between arcs in each set were fixed. Then all the data in each set were adjusted, according to the calibrations. We started with a baseline solution (LGM-296a) that included all the data. Eleven subset solutions were computed with respect to LGM-296a, complete to degree and order 70. The calibration factors were calculated as per equations (8) and (9). The final calibrated solution (GLGM-2) was derived using the calibration factors derived from all 11 subset solutions.

Comparison of the RMS degree variance for the GLGM-2 coefficients and coefficient sigmas indicates that the coefficient sigmas have greater power than the coefficients themselves for degrees $l \geq 30$. As a consequence, the calibration factors were calculated by averaging the K_l (from equation (9)) only through degree 30. Most of the calibration factors are already close to unity and indicate that the a priori weights selected for the data were approximately correct and that there is no set of data that grossly distorts the solution. No reasonable calibrations were derived for the high altitude periapsis data from Lunar Orbiter 4, so the calibrations from LO-4 set 2 were applied to the LO-4 set 1 data. The LO-4 set 1 data are extremely weak because of the high periapsis height (2700 km), relatively long period (6 hours), and numerous attitude maneuvers. The final calibration factors used to derive GLGM-2 from the base model (LGM-296a) are summarized in Table 5. For completeness, we show a complete table of the final sigmas applied to the data in GLGM-2, following the calibration procedure (see Table 6).

Table 5. Calibration Factors for the Doppler Data in GLGM-2

Satellite Data	Description	Calibration
LO-5		1.245
LO-4, set 1	Primary mission.	...
LO-4, set 2	Extended mission.	1.252
LO-2, set 1	Primary mission, $i = 12°$.	1.362
LO-2, set 2	Extended mission, $i = 17°$.	1.629
LO-3, set 1	Primary and extended mission (eccentricity = 0.28 to 0.33).	1.553
LO-3, set 2	Extended mission (eccentricity = 0.04).	1.818
LO-1		2.761
Clementine		1.523
A-15ss[a]		1.530
A-16ss[a]		1.175

[a] A-15ss = Apollo 15 subsatellite. A-16ss = Apollo 16 subsatellite.

Results

Power of the Coefficients

The coefficient variances at degree l, $\sigma_l(U)$, can be represented according to the convenient relation from *Kaula* [1966]:

$$\sigma_l(U) = \left[(2l+1)^{-1} \sum_{m=0}^{l} (\bar{C}_{lm}^2 + \bar{S}_{lm}^2)\right]^{1/2} \tag{12}$$

The coefficient degree variances, for the *Konopliv et al.* [1993] field, and for GLGM-2 are shown in Figure 2. The coefficient degree variances are compared with the signal of the power law applied in these gravity solutions, of $15 \times 10^{-5}/l^2$. The *Konopliv et al.* [1993], Lun60d, field has power considerably in excess of the power law. In contrast, the coefficient power of GLGM-2 at the higher degrees is strongly attenuated and falls below the power law. The coefficient variances for LGM-309c are also shown to illustrate the effect of omitting the application of the Kaula constraint in the GLGM-2 solution. Solutions without a Kaula constraint, where $l_{max} \geq 30$, simply would not invert. It is apparent, even in truncating the solution at $l = 30$, the high-degree terms develop excessive and unreasonable power. Comparison of the GLGM-2 and the LGM-309c solutions shows that the power law constraint has a noticeable effect starting at about degree 18. We note that most of the gravitational power associated with the major mascon basins falls at degrees 10-12, where the power law does not have significant influence. Thus interpretations about the long wavelength compensation state of the Moon [*Zuber et al.*, 1994] based on a preliminary version of this gravitational model are supported by more detailed analysis of the gravity.

The coefficient sigma degree variances from GLGM-2, Lun60d, and LGM-309d (GLGM-2 with no Clementine data) are illustrated in Figure 3. The scale difference in the coefficient sigmas between the *Konopliv et al.* [1993] Lun60d field and GLGM-2 generation of models is due to different schemes used to weight the data. *Konopliv et al.* [1993] weighted data closer to the RMS of fit, which overall was of the order of a few

Table 6. Final Sigmas Assigned to Data Used in the GLGM-2 solution

Data	Description	Number of Arcs	Number of Observations	Data Sigma cm/s
LO-1	Primary and extended mission.	42	39,885	2.76
LO-1	Extended mission. Includes 10-day arc (Sept. 22 to Oct. 1, 1966).	6	4,618	5.52
LO-2	Primary mission (Nov. 10 to Nov. 30, 1966).	10	32,226	1.36
LO-2	Primary mission (Dec. 1 to Dec. 7, 1966).	13	17,389	2.72
LO-2	Extended mission, set A[a]	32	19,975	1.63
LO-2	Extended mission, set B[a]	20	6,831	2.82
LO-3	Primary mission (Feb. 12, to Feb. 23, 1967).	12	19,368	3.11
LO-3	Primary mission (Feb. 24, to Mar. 7, 1967).	18	9,926	2.69
LO-3	Extended mission, set A[a]	3	1,164	1.55
LO-3	Extended mission, set B[a]	7	4,459	4.66
LO-3	Extended mission multiday arcs.	4	14,861	15.53
LO-3	Near circular orbit (Sept. 1967).	11	4,385	1.82
LO-4	Primary mission (May 1967).	5	32,551	3.33
LO-4	Extended mission (June 1967).	6	16,183	1.25
LO-5	Primary mission (Aug. 5 to Aug. 19, 1967).	16	17,393	1.25
LO-5	Primary mission (Aug. 19 to 22, 1967): 3-day arc.	1	5,673	1.25
LO-5	Primary mission (Aug. 22, 1967).	1	763	5.57
LO-5	Primary mission (Aug. 23 to 24, 1967).	1	1,797	2.48
LO-5	Primary mission (Aug. 26, 1967).	3	1,657	3.74
LO-5	Extended mission (Oct. 1, 1967 to Jan. 29, 1968).	29	20,407	1.25
A-15ss[b]	Sparse tracking. 2-3 day arcs.	11	2,940	4.59
A-15ss[b]	Sparse tracking. 1-day arcs.	20	4,033	3.06
A-15ss[b]	Sept., Oct., Dec., 1971 gravity campaigns.	50	37,123	2.16
A-16ss[b]		35	31,453	3.53
Clementine		36	361,794	1.36

[a] LO-2 and LO-3 extended mission data (set A) includes those arcs that had documented attitude maneuvers. LO-2 and LO-3 extended mission data (set B) includes those arcs with no documented attitude maneuvers.
[b] A-15ss = Apollo 15 subsatellite; A-16ss = Apollo 16 subsatellite.

mm/s. The intention of this approach was to minimize Doppler residuals to produce a model optimized for orbit prediction. In contrast, the a priori weights in GLGM-2 were approximately 1 cm/s, and the data were further downweighted in the calibration procedure. Our approach was to minimize systematic sources of error in the force and measurement models that have a tendency to produce striping correlated with satellite

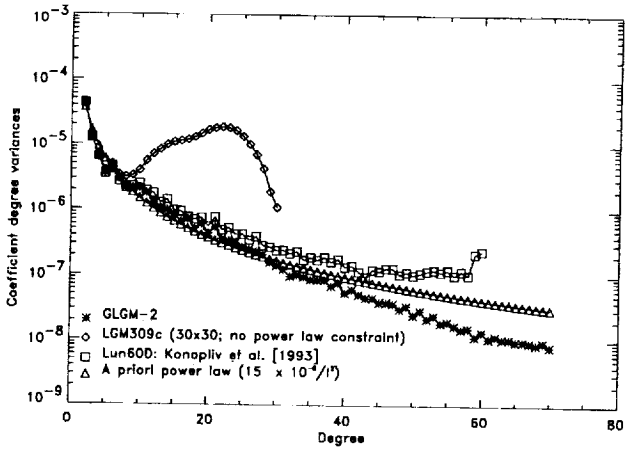

Figure 2. Comparison of coefficient degree variances for GLGM-2, the *Konopliv et al.* [1993] solution, and LGM-309c, a solution complete to degree and order 30 derived with no Kaula constraint.

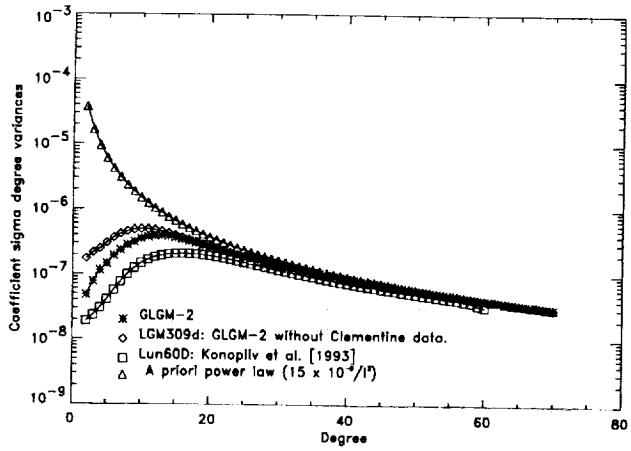

Figure 3. Comparison of coefficient sigma degree variances for GLGM-2, the *Konopliv et al.* [1993] solution, the LGM-309d, a solution complete to degree and order 70 without the Clementine data.

orbital ground tracks. Such structures are irrelevant for orbit prediction applications, but they are nonphysical and may mask subtle signals that could contain information on the internal density distribution of the planet. Our approach for data weighting was driven by a desire to produce a gravity field useful for lunar geophysics which manifests, to the extent possible, a realistic pattern of gravity anomalies when mapped onto the lunar surface.

Description of the Solution

Gravity anomalies from GLGM-2. The solution is complete to degree and order 70, corresponding to a half wavelength resolution of approximately 2.6° (80 km), where there is adequate data coverage. When evaluated at the surface with a reference radius of 1738 km, and after removing the appropriate hydrostatic terms, free-air gravity anomalies have a range of -294 to +358 mGals. The anomalies from GLGM-2 are depicted in Plate 1, and the projected errors from the gravity field error covariance are shown in Figure 4. The range in the free-air gravity anomalies is smaller in GLGM-2 than in the *Konopliv et al.* [1993] solution, which has a range of -454 to 529 mGals. The reason for the difference is that the power of the high-degree terms of GLGM-2 was attenuated to avoid the excessive orbit striping evident in the Lun60d model, when the gravity anomalies were downward continued to the surface of the planet. Consequently, GLGM-2 underestimates the expected power in the lunar gravity field at short wavelengths.

The projected errors, depicted in Figure 4, range from 17 to 20 mGals on the equatorial nearside (where the densest, low-altitude tracking data were obtained) to 45 mGals on the high-latitude regions of the farside. The 33 mGal contour essentially bounds the region where direct tracking of the Apollo 15 subsatellite was obtained.

GLGM-2 shows that the lunar highlands are generally characterized by low amplitude gravity anomalies that indicate a state of isostatic equilibrium, consistent with the highlands' age and origin as a near-global geochemical melt product [*Wood et al.*, 1970]. The model resolves the major nearside mass concentrations or "mascons," represented as large positive gravity anomalies, first deduced from Lunar Orbiter tracking more than 20 years ago [*Muller and Sjogren*, 1968]. The major mascons include Imbrium, Serenitatis, Crisium, Smythii, and Humorum. The mascon anomalies are attributed to a combination of the gravitational attraction of mare fill and to uplift of the lunar Moho associated with the impact process.

GLGM-2 also resolves gravitational lows or moats surrounding the major mascon basins on the nearside, such as Imbrium, Serenitatis, Crisium, and Humorum. After careful consideration, we are certain these features are genuine features of the lunar gravity field, as opposed to artifacts associated with "ringing" in the spherical harmonic solution. They occur on the nearside, in regions where there are independent tracks from several satellites. In fact, *Muller and Sjogren* [1968] noted the presence of these lows in their analysis of the Lunar Orbiter data, but their observation received little attention. Later, *Muller et al.* [1974] reported the existence of lows surrounding Serenitatis and Crisium in their analysis of the S band tracking of the Apollo 15 command module, which came to within 12 km of Serenitatis. In a separate analysis [*Neumann et al.*, 1997] we reanalyzed Lunar Orbiter LOS Doppler data and independently verified the presence of the annular lows. These negative rings are much more conspicuous in our model than in previous spherical harmonic representations of the lunar gravity field, in part because of greater surficial coverage provided by Clementine at mid to high nearside latitudes, but also because our field is evaluated at the surface rather than spacecraft altitude. We originally interpreted these annular rings to be a consequence of lithospheric flexure in response to surface loading of the lunar lithosphere by the maria [*Zuber et al.*,, 1994]. However, subsequent analysis [*Williams et al.*, 1995], which considered flexural effects of both surface maria loading and subsurface loads associated with crustal thinning, indicates that anomaly amplitudes are in nearly all cases too large to be explained by flexure alone. Similarly, the anomaly magnitudes would require unrealistic amounts of brecciation to be attributed solely to ejecta fallback. Our revised interpretation is that these features represent crustal thickening related to basin formation or modification [*Neumann et al.*, 1996], but our hypothesis has yet to be tested quantitatively.

Mare Orientale, with an age of 3.8 billion years is the youngest of the major lunar impact basins, shows a central mascon with a maximum amplitude of 188 mGals, surrounded by a horse-shaped gravitational low centered on the Inner and Outer Rook rings. The maximum amplitude of the bounding low is -275 mGals, but its variability in shape and amplitude do not correlate with surface topography (K.K. Williams and M.T. Zuber, manuscript in preparation, 1997) and so represents evidence for significant subsurface structural heterogeneity. The Mendel-Rydberg basin, just to the south of Orientale, is barely resolved, with a low of approximately 22 mGals. Since Mendel-Rydberg has considerable topographic relief (6 km from rim to floor [*Smith et al.*, 1997]), the lack of a significant gravity anomaly suggests this feature is almost fully compensated [*Zuber et al.*, 1994].

On the lunar farside, South Pole-Aitken is resolved as a gravity low, with minima near Van de Graff (25°S, 185°E, -116 mGals), Apollo (44°S, 212°E, -102 mGals), and Antoniadi (75°S 180°E, -82 mGals). Given the amplitude of the anomaly compared to the basin depth of 12 km [*Zuber et al.*, 1994], South Pole-Aitken must be approximately 90% compensated; however, deviations from compensation may well be a consequence of the younger, smaller basins within its confines [*Neumann et al.*, 1996].

The GLGM-2 model resolves other farside basins such as Hertzsprung, Mendeleev, Tsiolkovsky, Moscoviense, and Freundlich-Sharonov. These basins, which do not

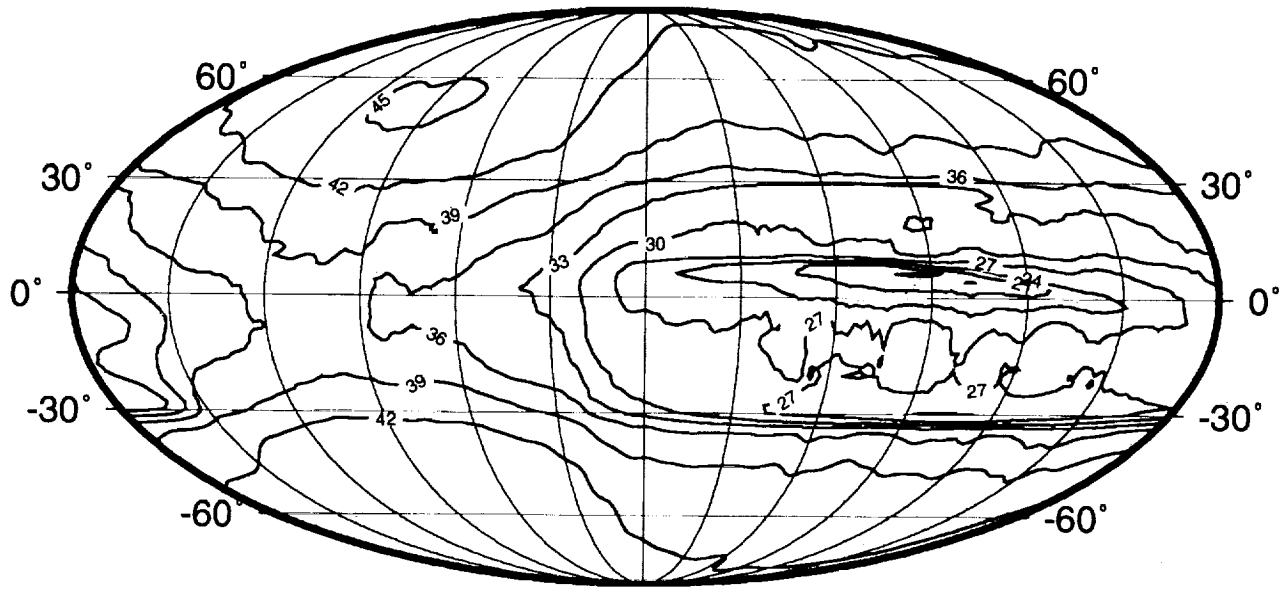

Figure 4. Projected gravity anomaly errors for GLGM-2, computed from the 70x70 error covariance. The map is a mollweide projection centered on 270°E longitude, and the contour interval is three mGals.

contain significant mare fill, are revealed as gravity lows (see Table 7), consistent with the findings of earlier investigators [*Ferrari*, 1977; *Ananda*, 1977]. A concentrated gravity high of 325 mGals is apparent directly north of Korolev at 4-5°N, 202°E. This high is located in a region which contains some of the highest topography on the Moon. The anomalies on the farside of the Moon sometimes appear stretched, compressed, or displaced from the known centers of the basins. For instance, both the centers of the gravity lows corresponding to Tsiolkovsky and Mendeleev are displaced 4° to the west of the basin center noted in lunar imagery. This smearing effect results from the lack of direct tracking over much of the far side of the Moon. While the association of anomalies with the farside basins is evidence that the Doppler data are sensitive to mass anomalies

Table 7. GLGM-2 Gravity Anomalies for Prominent Lunar Basins and Maria

Feature	Location	GLGM-2 Gravity Anomaly, mGals	GLGM-2 Anomaly Error, mGals	LGM-309b Anomaly,[a] mGals
Imbrium	341°E, 36°N	311	37	301
Crisium	58.5°E, 17°N	324	32	350
Mare Orientale	266°E, 19.5°S	188	29	211
Fecunditatis	52°E, 4°S	90	25	99
Nectaris	34°E, 16°S	274	29	281
Smythii	86.6°E, 2.4°S	173	28	170
Humorum	320.5°E, 24°S	318	27	321
Serenitatis	19°E, 26°N	356	33	340
Nubium	345°E, 21°S	-27	27	-37
Mendel-Rydberg	272°E, 52°S	22	41	-31
Freundlich-Sharonov	175°E, 18.5°N	-36	40	-12
Hertzsprung	231.5°E, 1.5°N	-87	33	-105
Moscoviense	147°E, 26°N	-56	41	-61
Korolev	203°E, 4.5°S	-48	36	-62
Mendeelev	141°E, 6°N	-169	37	-175
South Pole-Aitken				
	185°E 25°S	-116	40	-142
	212°E 44°S	-102	44	-115
	180°E 75°S	-82	44	-103

[a]The LGM-309b solution is a test solution that used the power law constraint of $30 \times 10^{-5}/l^2$. GLGM-2 used a power law constraint of $15 \times 10^{-5}/l^2$.

even in areas that lack direct tracking, it is quite certain that the gravity field does not accurately represent the anomaly amplitudes [cf. *Solomon and Simons*, 1996]. Consequently, geophysical analyses that incorporate regions without direct tracking data should be done with the greatest of caution.

A further characteristic of GLGM-2 is that the model exhibits greater detail in the equatorial regions than at higher latitudes. This variable resolution is a result of the orbital coverge of the satellites contributing data to GLGM-2 and is not an intrinsic feature of the lunar gravity field.

Contribution of Clementine. To assess the contribution of the Clementine data to the lunar gravitational field, we computed a spherical harmonic solution based only on these data and compared it to the full GLGM-2 solution. The free-air anomalies from the Clementine-only gravity solution (LGM-261), illustrated in Plate 2, have a range of -121 to 255 mGals (compared to -294 to +358 mGals for GLGM-2). Due to Clementine's polar orbit and global coverage, the Clementine data now provide the strongest satellite constraint on the long wavelength gravitational signature of the Moon. Various analyses presented in the following sections underscore the contribution of the Clementine data.

Comparison of the full GLGM-2 solution from Plate 1 with those from the Clementine-only solution (Plate 2) shows the extent to which the historic data are essential for adding detail to GLGM-2, particularly in the equatorial regions. Nonetheless, the major mascon basins can be discerned clearly from the Clementine data alone. Orientale appears as a broad low, although the mascon at the center is not resolved. The South Pole-Aitken basin appears as a broad low with a minimum of about -100 mGals. The Clementine-only free-air anomaly map also illustrates the presence of the low or moat, surrounding Imbrium (discussed above), which confirms its existence using data from a completely independent satellite. Artifacts in the handling of the Clementine data are apparent, as suggested by the vertical striping near 135°E longitude on the farside.

Error analysis. Gravity anomaly errors, as computed from the calibrated covariance of the GLGM-2 gravity solution, range from 17 mGals in the equatorial regions of the nearside to 45 mGals in the higher latitude regions of the lunar farside (see Figure 4). The error distribution correlates with the distribution of available tracking data (see Figure 1), and the proximity of periapsis to the lunar equator for the eccentric lunar orbiters. The gravity anomaly errors are listed in Table 7, along with the computed free-air gravity anomalies of prominent lunar basins and maria. The GLGM-2 gravity anomaly values are compared with those from LGM-309b, where the power law constraint was relaxed to $30 \times 10^{-5}/l^2$. Relaxing the power law constraint increases the power in the field. However, the anomalies computed from the LGM-309b field differ from the GLGM-2 values by less than the predicted GLGM-2 gravity anomaly uncertainty.

The lunar geoid. The geoid, computed from the GLGM-2 solution, is shown in Plate 3. The planet has a total range in geoid space of -275 to 475 m. This compares to total range of 200 m for the Earth and 2,000 m for Mars. Many lunar basins have prominent geoid signatures. There is a broad-scale correlation of geoid with topography (see Figure 5), with the exception of the mascon basins (cf. Imbrium, Serenitatis, Crisium, Humorum), which are geoid highs. Since these basins are located at lower elevations, and since the total elevation change over these basins is small compared to the total range in planetary topography, these mascon basins appear as spikes in Figure 5. South Pole-Aitken is revealed as a large and prominent geoid low with a minimum of about -270 m. The uncertainty in the GLGM-2 geoid also correlates with the tracking data distribution and is nearly identical in shape to the free-air gravity anomaly error map, depicted in Figure 4. The projected errors from the GLGM-2 error covariance range from 2 m on the equatorial nearside to 24 m on the high latitude regions of the farside.

Tests With the RMS of Fit

A series of test arcs involving each satellite in the gravity solution were selected to evaluate the performance of the interim solutions. The RMS of fit was computed for these arcs for the a priori *Konopliv et al.* [1993] field, the GLGM-1 solution [*Lemoine et al.*, 1994], and the current solution, GLGM-2. The results are summarized in Table 8. The fit to the Lunar Orbiters 2, 4, and 5 are the same as with the *Konopliv et al.* [1993] 60th degree and order model. We show slight improvements in the orbital tests with Lunar Orbiter 1 and the Apollo 15 subsatellite and obtain a higher RMS of fit for both the Apollo 16 subsatellite and Lunar Orbiter 3. We attribute the somewhat higher fit on the Apollo 16 subsatellite to the initial a priori weight for these data (3 cm/s). This weight was selected since this satellite was tracked at altitudes of less than 30 km just prior to impacting the Moon aat the end of May 1972. It appears now in retrospect that a higher a priori weight would have been justified (i.e. 1 cm/s), especially since these data were processed in arcs of only a few hours in length.

For short arcs (1 to 2 days) of Clementine data, we saw little difference in the RMS of fit to the tracking data when using either a priori *Konopliv et al.* [1993] model, and both GLGM-1 and GLGM-2. For this reason, our test set of Clementine arcs are longer - between 4 and 12 days in length. As would be expected, once the data are added into GLGM-1 and GLGM-2, we see an improved fit on these test arcs, compared to the *Konopliv et al.* [1993] model.

Analysis of Coefficient Differences

The differences in the coefficient sigmas between GLGM-2 and Lun60d [*Konopliv et al.*, 1993], normalized by the coefficient sigmas from the GLGM-2 gravity model are shown in Figure 6. These coefficient differ-

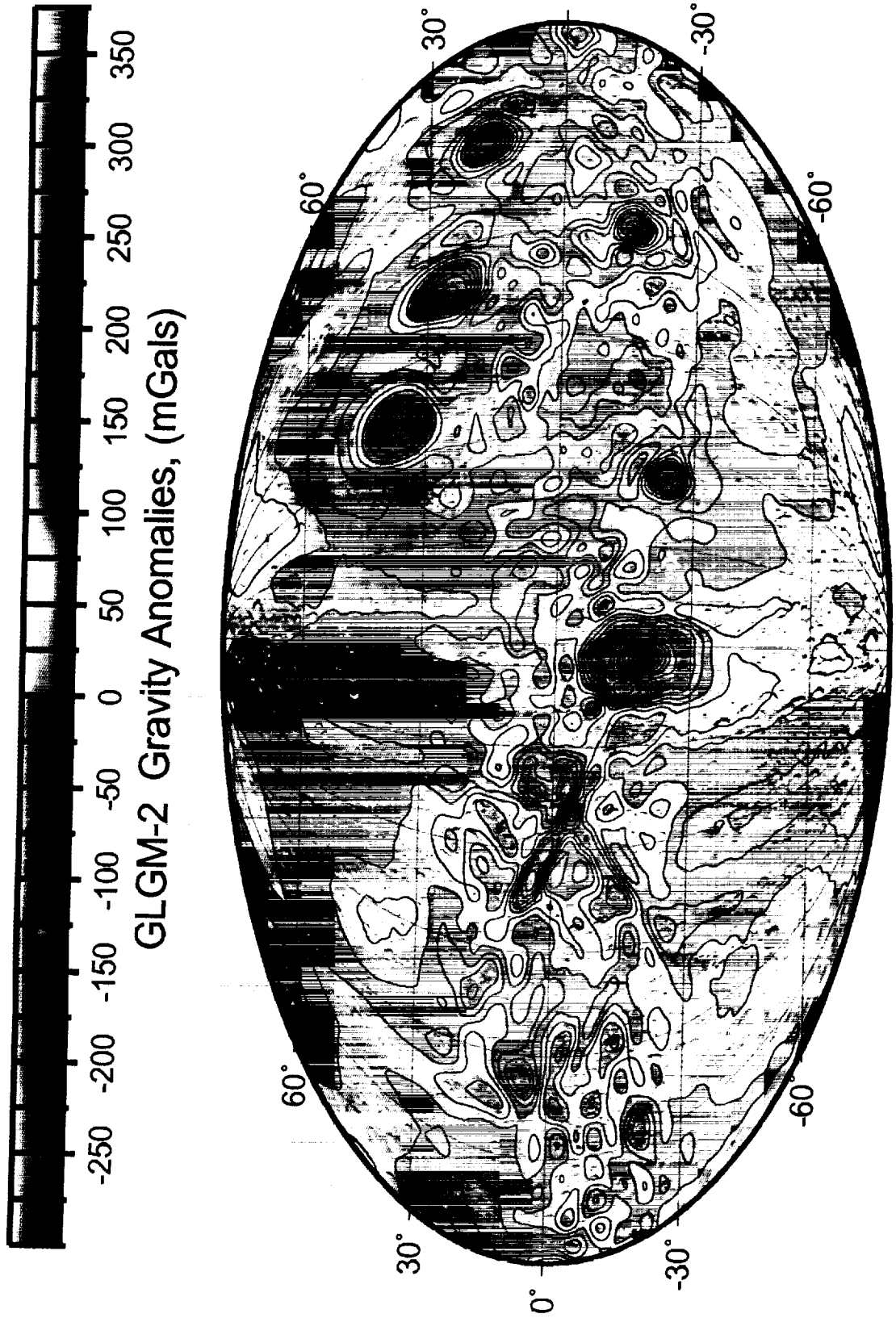

Plate 1. Lunar free-air gravity anomalies from GLGM-2, computed with respect to a reference radius of 1738.0 km, and an inverse flattening $1/f$ of 3234.930 (essentially removing J_2). The map is a molleweide projection centered on 270°E longitude, with the farside of the Moon to the left of center, and the nearside of the Moon to the right of center. The gravity anomalies are overlain on a digital shaded relief map of the lunar surface. The contour interval is 50 mGals.

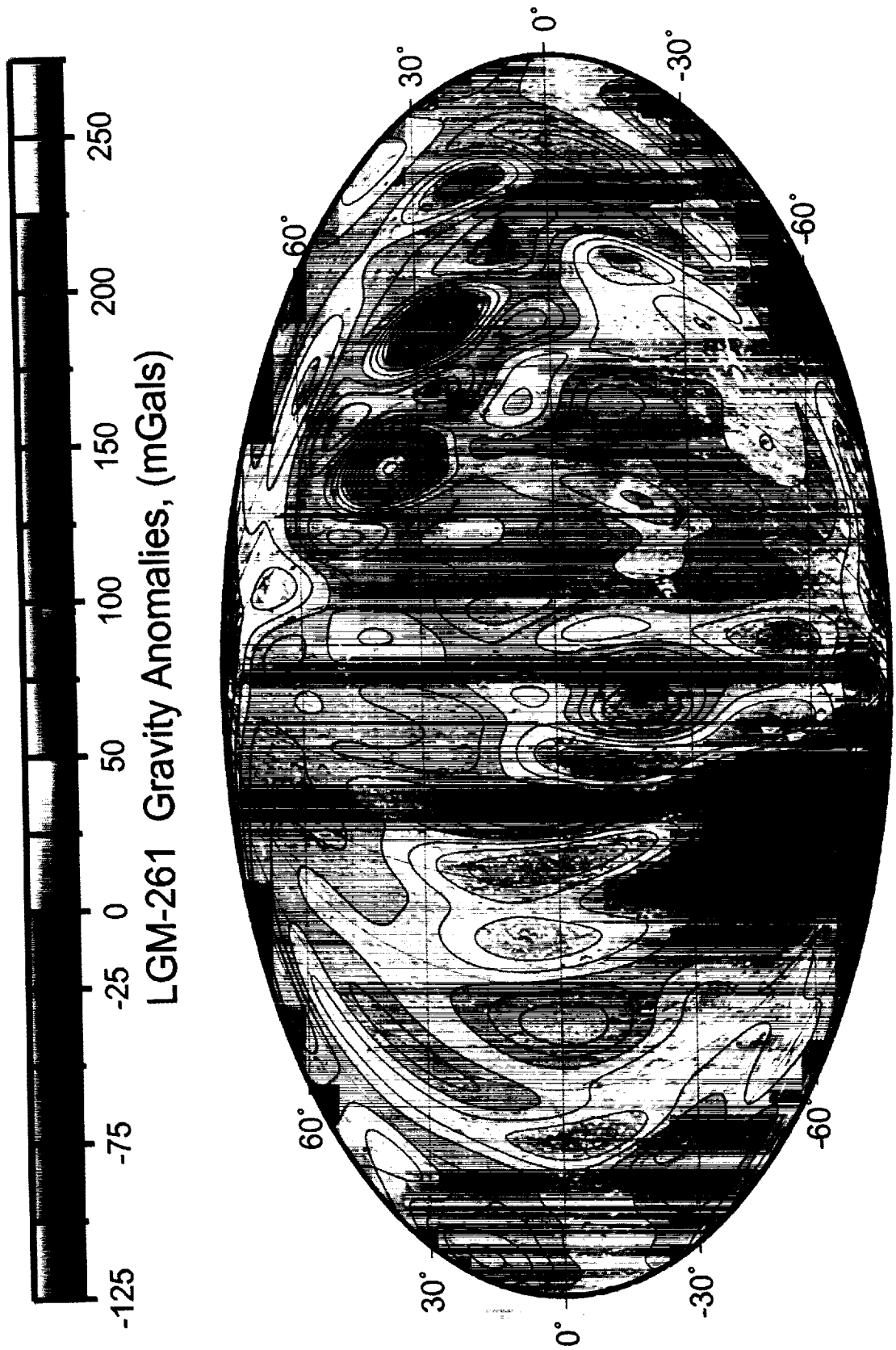

Plate 2. Lunar free-air gravity anomalies from LGM-261, a gravity solution based solely on the Clementine data, computed with respect to a reference radius of 1738.0 km, and an inverse flattening $1/f$ of 3234.930. The map is a mollweide projection, centered on 270°E longitude, with the farside of the Moon to the left of center, and the nearside of the Moon to the right of center. The contour interval is 25 mGals.

Plate 3. Geoid computed from the GLGM-2 gravity solution shown on a mollweide projection, centered on 270°E longitude, computed by removing J_2 with respect to a reference radius of 1738.0 km. The geoid is overlain on a digital shaded relief map of the lunar surface. The contour interval is 50 m.

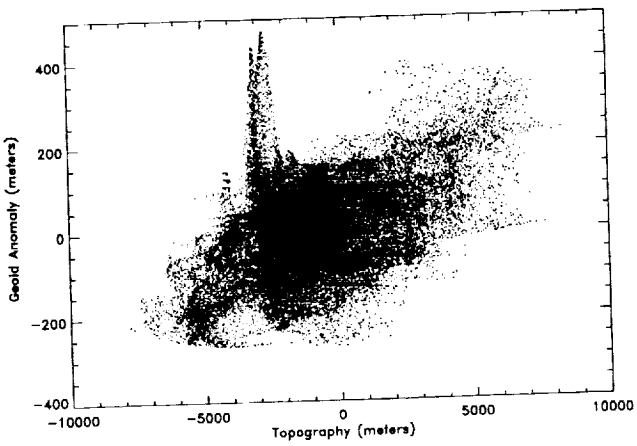

Figure 5. Geoid anomalies from GLGM-2 versus Clementine-derived topography [*Smith et al.*, 1997].

ences are compared to the solution without the Clementine data (LGM-309d). Concentrating on the field below degree 20, the figure shows that the Clementine data have the most profound effect on the lower degree portion of the field. In fact, the addition of Clementine changes the J_{22}, J_3, J_{31}, J_{33}, J_{42}, J_{44}, and the sectoral terms (the J_{lm} coefficients for which $l = m$) through degree 10, by three to nine sigma. In Figure 7, we illustrate the percent difference in the coefficient sigmas between the LGM-309d solution (no Clementine data) and the GLGM-2 solution. This figure illustrates the sensitivity of the Clementine data to the gravity field, and underscores the strength of this satellite's contribution to the low degree (l = 2 to 3), and sectoral terms through degree 20. The sectoral terms of the spherical harmonic expansion are purely longitudinal [*Kaula*, 1966]. The sensitivity that Clementine provides for these terms results from the polar orbit geometry of the spacecraft, as well as the strength and quality of the tracking data.

Of interest is to compare the solution for the low degree terms from GLGM-2 with those derived from lunar laser ranging. We present the comparisons in Table 9. The greatest discrepancies occur for J_3, C_{22}, and C_{31}. All other terms show reasonably close agreement. We also include in Table 9 the coefficients from LGM-309d (GLGM-2 with no Clementine data), to illustrate

Table 8. RMS of Fit Tests With Lunar Gravity Models

Gravity Field	Spacecraft	Number of Arcs	Average Arc Length, hrs	Average RMS of fit, cm/s
Lun60d[a]	LO-5	7	148.04	0.151
GLGM-1[b]				0.172
GLGM-2[c]				0.155
Lun60d	LO-4	7	98.8	0.065
GLGM-1				0.082
GLGM-2				0.071
Lun60d	LO-3	12	25.08	0.098
GLGM-1				0.207
GLGM-2				0.284
Lun60d	LO-2	11	38.98	0.146
GLGM-1				0.148
GLGM-2				0.147
Lun60d	LO-1	5	86.17	0.230
GLGM-1				0.111
GLGM-2				0.150
Lun60d	A-15ss[d]	26	82.67	2.185
GLGM-1				2.041
GLGM-2				1.915
Lun60d	A-16ss[d]	36	4.48	0.115
GLGM-1				1.221
GLGM-2				0.158
Lun60d	Clementine	5	206.40	0.296
GLGM-1				0.087
GLGM-2				0.093

[a] 60x60 spherical harmonic solution from *Konopliv et al.* [1993].
[b] 70x70 spherical harmonic solution from *Lemoine et al.* [1994].
[c] 70x70 spherical harmonic solution from this paper.
[d] A-15ss = Apollo 15 subsatellite. A-16ss = Apollo 16 subsatellite.

Coefficient differences between GLGM-2 and LUN60D, normalized by the sigmas from GLGM-2

Degree	0	1	2	3	4	5	6	7	8	9	10	11	12
2		1.4	1.4	4.7									
3	7.2	3.2	0.0	4.9									
4	0.3	1.8	4.4	0.4	9.7								
5	2.7	3.1	1.3	0.3	0.8	9.2							
6	1.7	0.8	0.2	0.3	2.2	0.8	9.4						
7	4.0	1.4	0.0	0.8	0.1	3.2	0.6	4.8					
8	0.0	0.6	2.2	0.4	0.9	0.2	0.6	0.2	6.3				
9	2.5	2.4	1.2	2.6	1.4	0.6	0.0	1.1	1.4	8.3			
10	3.7	0.2	2.4	0.8	2.5	0.2	1.6	0.4	6.3	2.8	6.0		
11	1.2	0.1	1.3	0.6	0.4	1.5	1.5	2.3	1.2	0.9	4.1	0.4	
12	2.0	0.8	1.6	1.1	0.6	1.1	1.8	2.8	2.1	2.2	2.1	3.4	0.2

Spherical Harmonic Order

Coefficient differences between LGM-309D and LUN60D, normalized by the sigmas from GLGM-2

Degree	0	1	2	3	4	5	6	7	8	9	10	11	12
2	0.5	1.1	0.2										
3	0.5	0.6	0.4	0.7									
4	1.2	0.4	0.4	0.2	0.1								
5	1.8	0.1	0.4	1.1	0.1	0.2							
6	0.9	1.1	1.5	0.0	1.1	0.1	0.3						
7	0.2	0.0	0.2	1.3	0.6	1.1	0.1	1.1					
8	0.5	0.0	0.2	0.3	0.8	0.5	0.2	0.2	0.4				
9	0.2	0.1	0.2	1.6	0.3	0.3	0.1	0.4	0.7	1.7			
10	1.8	0.1	1.3	0.3	0.8	0.6	1.6	0.3	3.2	2.3	1.8		
11	1.1	0.2	0.7	1.6	0.3	1.1	1.4	2.1	1.1	0.9	3.0	1.8	
12	0.5	0.5	1.4	0.8	1.3	0.6	1.2	2.3	2.4	2.1	2.2	2.1	0.9

Spherical Harmonic Order

Figure 6. Coefficient differences between Lun60d [*Konopliv et al.*, 1993] and GLGM-2, normalized by the sigmas from GLGM-2.

the influence of Clementine on these low degree terms. Comparison of the coefficients for J_3 and C_{22} shows that it is the Clementine data that change their estimates so strongly. The strength of these determinations results in part from the multiday arcs (4, 6, 10, and 12 days) used to process the Clementine tracking data. C_{31} is the most weakly determined of the low-degree terms determined by lunar laser ranging (LLR), and the C_{31} coefficients derived from the satellite determined gravitational models agree more with each other than with the LLR-determined value.

GM Determination

GLGM-2 included an adjustment for the lunar GM, and we obtained 4902.80295 ± 0.00224 km^3/s^2. The GLGM-2 estimate is compared with other values in Table 10. The *Ferrari et al.* [1980] value of 4902.7993 ± 0.0029 km^3/s^2 is determined largely from the high-altitude tracking of the Lunar Orbiter 4 spacecraft. The small sigma for the lunar GM in GLGM-1 is caused by the over optimistic sigma applied to the Clementine Doppler data in that model of 0.50 cm/s. In contrast, the sigma on the lunar GM in GLGM-2 is derived from a calibrated solution, where the Clementine data received an effective final data sigma of 1.36 cm/s. The differences between the various lunar GM determinations are a few parts in 10^7.

Covariance Analyses

Gravity field error versus order. We have projected the the 70x70 error covariance of the GLGM-2 gravity solution onto lunar spacecraft orbits, using the ERODYN covariance propagation software [*Englar et al.*, 1978]. We mapped the uncertainties and correlations for each spherical harmonic order on near-circular polar orbits (inclination of 89°) at altitudes of 25, 50, 100, and 400 km. This information is summarized in Figure 8. *Kaula's* [1966] linear orbit perturbation theory predicts that the order 1 and order 2 m-daily perturbations, with periods of approximately 28 and 14 days, will produce the largest perturbations on the spacecraft

Degree	0	1	2	3	4	5	6	7	8	9	10	11	12	13	14	15	16	17	18	19	20
2	72	60	82																		
3	54	56	56	83																	
4	35	27	43	53	82																
5	25	61	24	44	52	80															
6	51	40	42	23	41	49	78														
7	39	35	44	44	24	42	46	74													
8	29	29	36	42	39	22	40	43	69												
9	29	40	32	33	40	34	19	37	39	62											
10	23	27	29	27	29	33	28	16	33	35	55										
11	19	21	23	23	25	24	27	23	12	27	33	50									
12	16	19	16	18	18	17	18	19	18	9	22	32	47								
13	11	13	14	13	14	14	15	14	13	14	8	17	31	45							
14	7	8	8	9	10	10	11	11	11	10	12	8	14	29	42						
15	4	5	6	5	8	7	8	10	9	9	9	11	8	12	26	39					
16	2	3	3	4	4	5	5	7	9	7	8	8	9	7	9	22	35				
17	2	1	2	2	3	3	4	4	6	7	6	7	7	8	7	8	18	30			
18	1	1	1	1	1	2	2	3	3	5	6	5	6	6	6	6	6	14	25		
19	1	1	1	1	1	1	1	1	2	3	4	4	4	5	5	5	5	5	11	21	
20	1	0	1	1	1	1	1	1	1	2	2	3	3	4	5	5	4	5	5	9	17

Spherical Harmonic Order

Figure 7. Percent change in the coefficient sigmas for GLGM-2 and LGM-309d (GLGM-2 with no Clementine data), normalized by the sigmas from LGM-309d.

Table 9. Comparison of Low Degree and Order Harmonics From Satellite Tracking and Lunar Laser Ranging

Coefficient[a]	LLR[b]	Lun60d[c]	GLGM-2[d]	LGM-309d[e]
J_2	204.0 ± 1.0	203.805 ± 0.057	203.986 ± 0.131	203.566 ± 0.467
J_3	8.66 ± 0.16	8.25 ± 0.06	9.99 ± 0.24	8.53 ± 0.53
C_{22}	22.50 ± 0.11	22.372 ± 0.011	22.227 ± 0.023	22.413 ± 0.130
C_{31}	32.4 ± 2.4	28.618 ± 0.018	28.290 ± 0.098	28.736 ± 0.179
S_{31}	4.67 ± 0.73	5.87 ± 0.02	5.54 ± 0.07	6.15 ± 0.21
C_{32}	4.869 ± 0.025	4.891 ± 0.009	4.886 ± 0.030	4.855 ± 0.075
S_{32}	1.696 ± 0.009	1.646 ± 0.008	1.656 ± 0.029	1.618 ± 0.064
C_{33}	1.73 ± 0.050	1.719 ± 0.003	1.756 ± 0.007	1.673 ± 0.038
S_{33}	-0.28 ± 0.020	-0.211 ± 0.003	-0.270 ± 0.006	-0.268 ± 0.035

[a] All coefficients are unnormalized.
[b] Lunar laser ranging (LLR) from *Dickey et al.* [1994].
[c] 60x60 spherical harmonic solution from *Konopliv et al.* [1993].
[d] 70x70 spherical harmonic solution from this paper.
[e] LGM-309d = GLGM-2 with no Clementine data.

orbit (see Figure 8). For a 100-km near-circular polar orbit, the total position error caused by uncertainties in the GLGM-2 gravity field will be 1.4 km at order 1 and 1.6 km at order 2. It is only beyond order 15 that the position uncertainty due to gravity field error falls below 100 m. In a 100-km near-polar orbit, the total position error due to the uncertainties in the GLGM-2 gravity field is 2.5 km. This total position error increases to 4.2 km for a circular polar orbit at 50-km altitude, and 5.7 km for a polar orbit with a mean altitude of 25 km. These error projections do not include the omission error of the terms beyond degree 70. The actual gravity field induced orbit error would be larger than the values cited here, especially for the lowest altitude orbits.

Projected orbit error versus inclination. Using the linear orbit theory of *Rosborough* [1986], the radial orbit error as predicted by the GLGM-2 covariance was mapped as a function of inclination, for a near-circular lunar orbit at an altitude of 100 km. The results are depicted in Figure 9. The radial error ranges from just over 122 m at 29° inclination to 1364 m at 129° inclination. The increase in projected error at the mid-range inclinations (30°to 140°) is understandable given that only data from predominantly low inclination satellites have contributed to GLGM-2. Careful examination of the spectrum also reveals that local minima occur near the specific inclinations from which satellite tracking data were acquired or at their complementary retrograde or prograde inclinations (11°, 21°, 29°, 80°, 90°, 100°, 151°, 159°, 169°). The data from the Apollo 15 subsatellite contribute strongly to GLGM-2, and it can be argued that the GLGM-2 field is strongly tuned to the orbit of the Apollo 15 subsatellite, since it has its lowest projected error at that satellite's inclination (151°, and its complement, 29°). Comparison of the predicted error from the GLGM-2 and the LGM-309d (solution with no Clementine data) reveals that Clementine reduces the gravity field error at the higher inclinations (60° to 140°) by 5-20%. At the inclination of 90°, Clementine reduces the radial orbit error from 743 to 554 m.

Summary

We have developed a spherical harmonic model of the lunar gravity field complete to degree and order 70 that incorporates the tracking data from Lunar Orbiters 1 to 5, the Apollo 15 and 16 subsatellites, and Clementine. The Clementine data provide the strongest satellite constraint on the low degree and order field, whereas the historic data are indispensable for providing distributed regions of high-resolution coverage within ±30°latitude. Our solution resolves the gravitational signatures of both farside and nearside basins and mascons. To stabilize the solution at short wavelengths that are not characterized by a globally uni-

Table 10. Comparison of Solutions for the Lunar GM

Analysis	Description	GM, km^3/s^2
Ferrari et al. [1980]	LLR and LO-4	4902.7993 ± 0.0029
Konopliv et al. [1993]	Lun60d (60x60)	4902.79781 ± 0.00122
Lemoine et al. [1994]	GLGM-1 (70x70)	4902.80263 ± 0.00095
This paper	GLGM-2 (70x70)	4902.80295 ± 0.00224
This paper	LGM-309d (70x70)	4902.80280 ± 0.00603

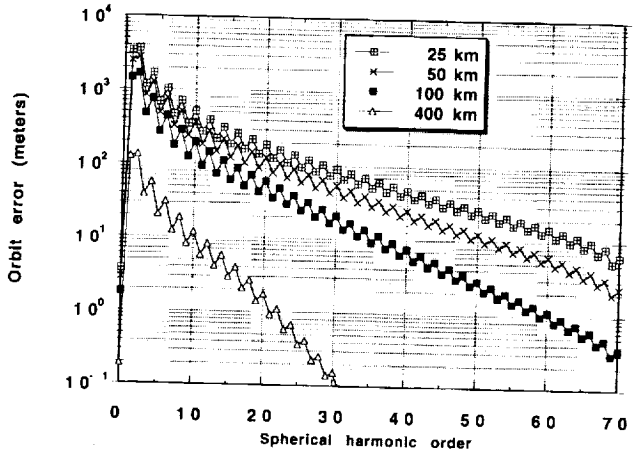

Figure 8. Projected total orbit error (1 sigma) from the 70x70 error covariance of GLGM-2 decomposed by gravity field order, for near-circular, polar, lunar orbits at 25 km, 50 km, 100 km, and 400 km altitude.

form data distribution, we applied an a priori power law of $15 \times 10^{-5}/l^2$. While use of this constraint was necessary in order to obtain the high degree and order solution, we note that GLGM-2 fails to exhaust the signal in the tracking data. Alternative gravity analysis techniques such as the mapping of LOS accelerations [*Kaula*, 1995; *Barriot et al.*, 1995] may be useful for extracting further information from the data, particularly on a regional basis in areas of dense, low altitude coverage. Although we believe GLGM-2 represents a significant improvement in the modeling of the lunar gravity field, particularly with regard to basin-scale structure, the fundamental problem in lunar geophysics remains the lack of global high resolution coverage. The Lunar Prospector mission is expected to improve significantly the spatial resolution over the mid- to high-latitude regions of the nearside. Nevertheless, a lunar mission that includes either satellite-to-satellite tracking or a gravity gradiometer to permit direct gravity mapping of the farside should remain a high priority for lunar science.

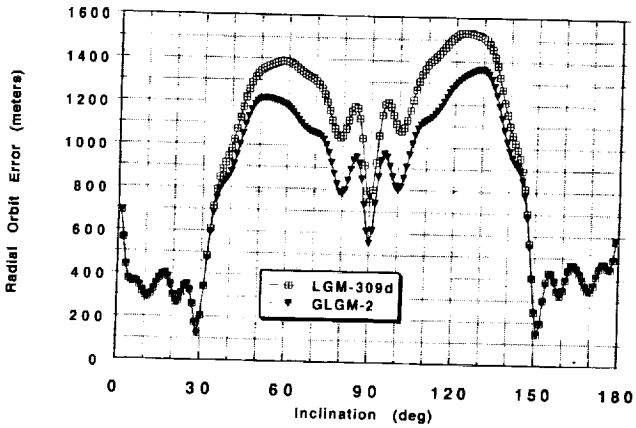

Figure 9. Radial orbit error (1 sigma) predicted from the 70x70 error covariances of the GLGM-2 and LGM-309d (GLGM-2 with no Clementine data) gravity solutions for near-circular 100 km altitude lunar orbits. This radial orbit error is shown as a function of orbit inclination.

Acknowledgments. We thank W. M. Kaula for a helpful review; W. L. Sjogren and A. S. Konopliv for providing the Lunar Orbiter and Apollo subsatellite data; the Clementine Operations Team at the Naval Research Lab and at the DSPSE Mission Operations Center including B. Kaufmann and J. Middour for providing ancillary information related to Clementine; R. M. Beckman, and the Goddard Flight Dynamics Facility for transmission of the Clementine data during the mission; J. A. Marshall (NASA GSFC) for valuable advice and technical support; S. K. Fricke (Hughes/STX and NASA GSFC) for data processing; E. J. O. Schrama (T. U. Delft, the Netherlands) for the use of his CGSST gravity anomaly error and geoid error mapping program; and G. W. Rosborough (University of Colorado, Boulder) for his SATRMS radial orbit error covariance propagation software. A portion of this analysis was performed on computer workstations originally obtained through the Mars Observer and Mars Global Surveyor Programs.

References

Ananda, M. P., Lunar gravity: A mass-point model, *J. Geophys. Res.*, 82(20), 3049-3064, 1977.

Anderson, K. A., L. M. Chase, R. P. Lin, J. E. McCoy, and R.E. McGuire, Subsatellite measurements of plasma and solar particles, Apollo 15 Preliminary Science Report, NASA Spec. Publ. *SP-289*, 21-1 to 21-14, 1972a.

Anderson, K. A., L. M. Chase, R. P. Lin,, J. E. McCoy, and R. E. McGuire, Subsatellite measurements of plasma and energetic particles, Apollo 16 Preliminary Science Report, NASA Spec. Publ. *SP-315*, 22-1 to 22-6, 1972b.

Barriott, J. P., G. Balmino, and N. Valès, Analysis of the LOS gravity data sets from cycles 5 and 6 of the Magellan probe around Venus (abstract), *Eos Trans. AGU, 76*(46), Fall Meet. Suppl., F331, 1995.

Bills, B. G., and A. J. Ferrari, A harmonic analysis of lunar gravity, *J. Geophys. Res., 85*(B2), 1013-1025, 1980.

Blackshear, W. T., and J. P. Gapcynski, An improved value of the lunar moment of inertia, *J. Geophys. Res., 82*, 1699-1701, 1977.

Bryant, W. C., and R. G. Williamson, Lunar gravity analysis results from Explorer 49, AIAA Paper 74-810, presented at the AIAA Mechanics and Control of Flight Conference, Am. Inst. of Aeronautics and Astronautics, Anaheim, Calif., Aug. 1974.

Chao, C. C., The troposphere calibration model for Mariner Mars 1971, in Tracking System Analytic Calibration Activities for the Mariner Mars 1971 Mission, *JPL Tech. Rep. 32-1587*, Jet Propulsion Lab., Pasadena, Calif., March 1, 1974.

Coleman, P. J., Jr., C. T. Russell, L. R. Sharp, and G. Schubert, Preliminary mapping of the lunar magnetic field, *Phys. Earth Planet. Inter., 6*, 167-174, 1972.

Davies, M. E., V. K. Abalakin, A. Brahic, M. Bursa, B. H. Chovitz, J. H. Lieske, P. K. Seidelmann, A. T. Sinclair, and Y. S. Tjuflin, Report of the IAU/IAG/COSPAR working group on cartographic coordinates and rotational elements of the planets and satellites: 1991, *Celest. Mech. and Dyn. Astron., 53*, 377-397, 1992.

Dickey, J. O., P. L. Bender, J. E. Faller, X X Newhall, R. L. Ricklefs, J. G. Ries, P. J. Shelus, C. Veillet, A. L. Whipple, J. R. Wiant, J. G. Williams, and C. F. Yoder, Lunar laser ranging: A continuing legacy of the Apollo program, *Science, 265*, 482-490, 1994.

Englar, T. S., R. H. Estes, D. C. Chinn, and G. A. Maslyar, ERODYN program mathematical description version 7809, *Bus. Technol. Syst. Contract. Rep.*, BTS-TR-78-69, NASA Goddard Space Flight Center, Greenbelt, Maryland, Sept. 1978.

Ferrari, A. J., Lunar gravity: A harmonic analysis, *J. Geophys. Res.*, *82*(20), 3065-3084, 1977.

Ferrari, A. J., W. S. Sinclair, W. L. Sinclair, J. G. Williams, and C. F. Yoder, Geophysical parameters of the Earth-Moon system, *J. Geophys. Res.*, *85*(B7), 3939-3951, 1980.

Folkner, W. M., Station locations for the Mars Observer encounter version of ODP, JPL interoffice memorandum, *Doc. IOM 335.1-93-013*, Jet Propulsion Laboratory, Pasadena, Calif., May 27, 1993.

Gapcynski, J. P., W. T. Blackshear, R. H. Tolson, and H. R. Compton, A determination of the lunar moment of inertia, *Geophys. Res. Lett.*, *2*(8) 353-356, 1975.

Hopfield, H. S., Tropospheric effect on electronmagnetically measured range: prediction from surface weather data, *Radio Sci.*, *6*(3), 357-367, 1971.

International Earth Rotation Service, 1993 IERS Annual Report, Central Bureau of the IERS, edited by M. Feissel and N. Essaifi, Observatoire de Paris, Paris, France, July 1994.

Kaula, W. M., *Theory of Satellite Geodesy*, Blaisdell, Waltham, Mass., 1966.

Kaula, W. M., A one-degree square mean, or 180th degree harmonic, solution for the gravitational field of Venus (abstract), *Eos Trans. AGU*, *76*(46), Fall Meeting Suppl., F331, 1995.

Konopliv, A. S., and W. L. Sjogren, Venus spherical harmonic gravity model to degree and order 60, *Icarus*, *112*, 42-54, 1994.

Konopliv, A. S., and W. L. Sjogren, The JPL Mars gravity model Mars50c based upon Viking and Mariner 9 Doppler tracking data, *JPL Publ. 95-5*, 73 pp, Jet Propulsion Laboratory, Pasadena, Calif., 1995.

Konopliv, A. S., W. L. Sjogren, R. N. Wimberly, R. A. Cook, and A. Vijayaraghavan, A high-resolution lunar gravity field and predicted orbit behavior, AAS Paper 93-622, presented at the AAS/AIAA Astrodynamics Specialist Conference, Victoria, British Columbia, Aug. 16-19, 1993.

Lawson, D. L., and R. J. Hanson, *Solving Least Squares Problems*, Prentice-Hall, Englewood Cliffs, N. J., 1974.

Lemoine, F. G., D. E. Smith, and M. T. Zuber, Goddard Lunar Gravity Model-1 (GLGM-1), A 70th degree and order gravity model for the Moon (abstract), *Eos Trans. AGU*, Fall Meeting Suppl., *75*(44), 400, 1994.

Lemoine, F. G., D. E. Smith, D. D. Rowlands, M. T. Zuber, G. A. Neumann, and N. K. Pavlis, The role of a priori contraints in the design of lunar gravity field solutions (abstract), *Eos Trans. AGU*, Fall Meeting Suppl., F152, *77*(46), 1996.

Lerch, F. J., Optimum data weighting and error calibration for estimation of gravitational parameters, *Bull. Geod.*, *65*, 44-52, 1991.

Lorell, J., and W. L. Sjogren, Lunar gravity: preliminary results from Lunar Orbiter, *Science*, *159*, 625-628, 1968.

Marsh, J. G., et al., A new gravitational model for the Earth from satellite tracking data: GEM-T1, *J. Geophys. Res.*, *93*(B6), 6169-6215, 1988a.

Marsh, J. G., et al., An improved model of the Earth's gravitational field: GEM-T1, *NASA Tech. Memo. 4019*, 1988b.

Marsh, J. G., et al., The GEM-T2 gravitational model, *J. Geophys. Res.*, *95*, 22,043-22,071, 1990.

Michael W. H. Jr., and W. T. Blackshear, Recent results on the mass, gravitational field and moments of inertia of the Moon, *Moon*, *3*, 388-402, 1972.

Moyer, T. D., Mathematical formulation of the Double Precision Orbit Determination Program (DPODP), *JPL Tech Rep. 32-1527*, Jet Propulsion Laboratory, Pasadena, Calif., May 15, 1971.

Moyer, T. D. Transformation from proper time on Earth to coordinate time in the Solar System barycentric space-time frame of reference, part I and part II, *Celest. Mech.*, *23*, 33-68, 1981.

Muller, P. M., and W. L. Sjogren, Mascons: Lunar mass concentrations, *Science*, *161*, 680-684, 1968.

Muller, P. M., W. L. Sjogren, and W. R. Wollenhaupt, Lunar gravity: Apollo 15 radio tracking, *Moon*, *10*, 195-205, 1974.

Nerem, R. S., J. McNamee, and B. G. Bills, A high resolution gravity model for Venus: GVM-1, *Geophys. Res. Lett.*, *20*, 599-602, 1993.

Nerem, R. S., F. J. Lerch, J. A. Marshall, E. C. Pavlis, B. H. Putney, B. D. Tapley, R. J. Eanes, J. C. Ries, B. E. Schutz, C. K. Shum, M. M. Watkins, S. M. Klosko, J. C. Chan, S. B. Luthcke, N. K. Pavlis, R. G. Williamson, R. H. Rapp, R. Biancale, and F. Nouel, Gravity Model Development for TOPEX/POSEIDON: Joint Gravity Models 1 and 2, *J. Geophys. Res.*, *99*(C12), 24,421-24,447, 1994.

Neumann, G. A., M. T. Zuber, D. E. Smith, and F. G. Lemoine, The lunar crust: global structure and signature of major basins, *J. Geophys. Res.*, *101*(E7), 16,841-16,863, 1996.

Neumann, G. A., F. G. Lemoine, and M. T. Zuber, What does graviy tell us about lunar crustal structure (abstract), *Lunar Planet. Sci. Conf. XXVIII*, 1713-1714, 1997.

Nozette, S. et al., The Clementine mission to the Moon: Scientific overview, *Science*, *266*, 1835-1839, 1994.

Pavlis, D. E., D. Moore, S. Luo, J. J. McCarthy, and S. B. Luthcke, GEODYN Operations Manual, 5 Volumes, Hughes/STX, prepared for NASA Goddard Space Flight Center, Greenbelt, Maryland, 1997.

Rosborough, G. W., Satellite orbit perturbations due to the geopotential, Ph.D thesis, The Univ. of Texas at Austin, Jan. 1986.

Sagitov, M. U., B. Bodri, V. S. Nazarenko, and Kh. G. Tadzhidinov, *Lunar Gravimetry*, Academic, San Diego, Calif., 1986.

Sjogren, W. L., P. Gottlieb, and P. M. Muller, Lunar gravity via Apollo 14 Doppler radio tracking, *Science*, *175*, 165-168, 1972a.

Sjogren, W. L., P. M. Muller, and W. R. Wollenhaupt, Apollo 15 gravity analysis from the S band transponder experiment, *Moon*, *4*, 411-418, 1972b.

Sjogren, W. L., R. N. Wimberly, and W. R. Wollenhaupt, Lunar gravity via the Apollo 15 and Apollo 16 subsatellites, *Moon*, *9*, 115-128, 1974a.

Sjogren, W. L., R. N. Wimberly, and W. R. Wollenhaupt, Lunar gravity: Apollo 16, *Moon*, *11*, 35-40, 1974b.

Sjogren, W. L., R. N. Wimberly, and W. R. Wollenhaupt, Lunar gravity: Apollo 17, *Moon*, *11*, 41-52, 1974c.

Smith D. E., F. J. Lerch, R. S. Nerem, M. T. Zuber, G. B. Patel, S. K. Fricke, and F. G. Lemoine, An improved gravity model for Mars: Goddard Mars Model 1, *J. Geophys. Res.*, *98*(E11), 20,871-20,889, 1993.

Smith, D. E., M. T. Zuber, G. A. Neumann, and F. G. Lemoine, Topography of the Moon from the Clementine Lidar, *J. Geophys. Res.*, *102*, 1591-1611, 1997.

Solomon, S.C., and M. Simons, The isostatic state of the lunar highlands from spatio-spectral localization of global gravity, topography and surface chemistry (abstract), *Lunar Planet. Sci. Conf.*, *XXVII*, 1245-1256, 1996.

Standish, E. M., Jr., The observational basis for JPL's DE200: The planetary ephemeris of the astronomical almanac, *Aston. Astrophys.*, *233*, 252-271, 1990.

Ullman, R. E., SOLVE Program: Mathematical formulation

and guide to user input, Hughes/STX contractor report, contract NAS5-31760, NASA Goddard Space Flight Center, Greenbelt, Maryland, 1994.

Williams, J. G., M. A. Slade, D. H. Eckhardt, and W. M. Kaula, Lunar physical librations and laser ranging, *Moon, 8,* 469-483, 1973.

Williams, J. G., X X Newhall, and J. O. Dickey, Lunar gravitational harmonics and reflector coordinates, in *Proceedings of the International Symposium on Figure and Dynamics of the Earth, Moon and Planets*, edited by P. Holota, pp. 643-648, Astronomical Institute of the Czechoslovak Academy of Sciences, Prague, 1987.

Williams, K. K., G. A. Neumann, and M. T. Zuber, Lunar mascon basins: Analysis of effective elastic thickness using gravity anomaly models (abstract), *Lunar Planet. Sci. Conf., XXVI,* 1505-1506, 1995.

Wong, L., G. Buechler, W. Downs, W. Sjogren, P. Muller, and P. Gottlieb, A surface layer representation of the lunar gravitational field, *J. Geophys. Res., 76*(26), 6220-6236, 1971.

Wood, J. A., J. S. Dickey Jr., U. B. Marvin, and B. N. Powell, Lunar anorthostites and a geochemical model for the Moon, *Geochem. Cosmochem. Acta, Suppl., 1,* 965-988, 1970.

Zuber, M. T., D. E. Smith, F. G. Lemoine, and G. A. Neumann, The shape and structure of the Moon from the Clementine mission, *Science, 266,* 1839-1843, 1994.

F. Lemoine, D. Rowlands, and D. Smith, Laboratory for Terrestrial Physics, NASA Goddard Space Flight Center, Greenbelt, MD 20771. (e-mail: flemoine@olympus.gsfc.nasa.gov; dave@usgrant.gsfc.nasa.gov; dsmith@tharsis.gsfc.nasa.gov)

G. Neumann and M. Zuber, Department of Earth, Atmospheric, and Planetary Sciences, Massachusetts Institute of Technology, Cambridge, MA 02138. (e-mail: neumann@tharsis.gsfc.nasa.gov; zuber@mit.edu)

(Received January 3, 1996; revised May 7, 1997; accepted May 17, 1997.)